High Power Laser Science and Engineering, (2024), Vol. 12, e71, 11 pages.
doi:10.1017/hpl.2024.40

HIGH POWER LASER SCIENCE AND ENGINEERING

RESEARCH ARTICLE

Performance enhancement in the long-wavelength low-gain region of Ti:sapphire lasers by an efficient stimulated Raman scattering process

Yuntao Bai[1,2], Xin Ding[1,2], Guoxin Jiang[1,2], Peng Lei[1,2], Ying Xie[1,2], Jiangeng Du[1,2], Yang Sun[1,2], Liang Wu[1,2], Guizhong Zhang[1,2], and Jianquan Yao[1,2]

[1] *Institute of Laser and Opto-electronics, School of Precision Instrument and Optoelectronics Engineering, Tianjin University, Tianjin, China*

[2] *Key Laboratory of Optoelectronic Information Technology (Ministry of Education), Tianjin University, Tianjin, China*

(Received 26 February 2024; revised 16 May 2024; accepted 17 June 2024)

Abstract

We demonstrated a method to improve the output performance of a Ti:sapphire laser in the long-wavelength low-gain region with an efficient stimulated Raman scattering process. By shifting the wavelength of the high-gain-band Ti:sapphire laser to the long-wavelength low-gain region, high-performance Stokes operation was achieved in the original long-wavelength low-gain region of the Ti:sapphire laser. With the fundamental wavelength tuning from 870 to 930 nm, first-order Stokes output exceeding 2.5 W was obtained at 930–1000 nm, which was significantly higher than that directly generated by the Ti:sapphire laser, accompanied by better beam quality, shorter pulse duration and narrower linewidth. Under the pump power of 42.1 W, a maximum first-order Stokes power of 3.24 W was obtained at 960 nm, with a conversion efficiency of 7.7%. Furthermore, self-mode-locked modulations of first- and second-order Stokes generation were observed in Ti:sapphire intracavity solid Raman lasers for the first time.

Keywords: folded coupled cavity; low-gain region; Raman laser; self-mode-locking; Ti:sapphire laser

1. Introduction

Ti:sapphire lasers with an output wavelength range of 660–1180 nm are important tunable laser sources and have been successfully demonstrated in various applications in the nuclear industry, laser spectroscopy, laser chemistry and laser remote sensing[1–3]. In particular, efficient tunable laser operation can always be readily achieved for 710–930 nm high-gain-band Ti:sapphire lasers with a stimulated emission cross-section slightly lower than that of the central wavelength at 795 nm (3×10^{-19} cm^2 @ 795 nm, 1.5×10^{-19} cm^2 @ 930 nm). In recent years, numerous studies on high-gain-band Ti:sapphire lasers have been conducted, including continuous-wave (CW), pulsed and mode-locked operations[4–7]. However, for the low-gain regions far from the central wavelength of Ti:sapphire lasers, such as 930–1180 nm, the maximum output powers are significantly lower than those of the high-gain regions because of the rapid decrease in the stimulated emission cross-section (7.7×10^{-20} cm^2 @ 1000 nm)[8–10]. This significant gain difference between the emission bands limits the advantages of Ti:sapphire lasers in wavelength tuning. Hence, the conversion efficiency of Ti:sapphire lasers must be enhanced in the low-gain region to ensure high-performance laser operation over the entire emission band.

The power enhancements of low-gain-band Ti:sapphire lasers typically rely on the loss control of Ti:sapphire lasers by optimizing the transmittances of the output coupler (OC), due to the limited laser gain. However, this method cannot fundamentally improve the gain of Ti:sapphire lasers within the low-gain region. Conventional Ti:sapphire amplification techniques do also not exhibit a significant advantage in this region, due to the limited seed power and extraction efficiency of the amplifier. In contrast, the nonlinear frequency conversion technique provides a new possibility to achieve efficient tunable Ti:sapphire laser operations in this region. By shifting the wavelength of the high-gain-band Ti:sapphire lasers to the low-gain region, higher gain of the Ti:sapphire lasers may be achieved in the low-gain region.

Correspondence to: X. Ding, Institute of Laser and Opto-electronics, School of Precision Instrument and Optoelectronics Engineering, Tianjin University, Tianjin 300072, China. Email: dingxin@tju.edu.cn

Therefore, efficient wavelength shifts within the gain bandwidth of Ti:sapphire lasers are crucial for enhancing the output performances of Ti:sapphire lasers in the low-gain region. Optical parametric oscillations (OPOs) can provide a widely tunable wavelength shift for Ti:sapphire lasers. However, such a short-wavelength shift between the high-gain and low-gain regions of the Ti:sapphire laser poses a challenge for OPOs. This necessitates additional nonlinear processes, which significantly reduces the conversion efficiency[11]. In contrast, stimulated Raman scattering (SRS) can perform the aforementioned task by a single Raman shift without phase matching. Therefore, we believe that it is possible to achieve efficient Raman operation in the original long-wavelength low-gain region of Ti:sapphire lasers by fully utilizing the high Raman gain. Moreover, the beam clean-up effect of SRS helps the Stokes wave achieve good beam quality, and the Stokes pulse also exhibits a significantly narrower pulse duration than the fundamental wavelength[12–14]. In conclusion, high-gain-band efficient Ti:sapphire Raman lasers have the potential to replace Ti:sapphire lasers, enabling high-performance tunable laser operations in their original low-gain region of 930–1180 nm.

In recent years, there have been few reports on Ti:sapphire Raman lasers[15–17]. In 2017, Kitzler *et al.*[15] reported a single-longitudinal-mode ring diamond Raman laser, which was resonantly pumped by a tunable CW single-mode Ti:sapphire laser. An 883 nm Stokes wave with an output power of 1 W was obtained at a pump power of 5 W at 790 nm. This study primarily focused on methods that yield a unidirectional Stokes operation. The feasibility of extending the output wavelength of Ti:sapphire lasers from 1.05 to 1.45 μm by using the cascade Raman process was also discussed. In 2020, Li *et al.*[16,17] improved this method to include a second Stokes operation and discussed the conditions for a single-longitudinal-mode output. A second-order Stokes wave (1101.3 nm) with a maximum output power of 0.364 W was obtained at a pump power of 3.86 W at 851.5 nm. Notably, the aforementioned reports on Ti:sapphire Raman lasers have mainly focused on techniques to achieve single-frequency Stokes operation. The Ti:sapphire laser was merely utilized as a high-quality tunable pump source, and the impact of the SRS process on the output performance of the Ti:sapphire laser was not a primary focus. However, we are primarily focused on exploring the utilization of the SRS process to achieve efficient laser operation in the long-wavelength low-gain region of Ti:sapphire lasers, thereby enhancing the output performance over the entire laser emission band. Relevant reports are very few, and theoretical or experimental evidence to prove that high-gain Ti:sapphire Raman lasers can be used to replace Ti:sapphire lasers to achieve high-performance tunable laser operations in the long-wavelength low-gain region is also unavailable.

In this study, we demonstrated a method to improve the output performance of a Ti:sapphire laser in the long-wavelength low-gain region with an efficient SRS process. By making full use of the high pump intensity in the intracavity Raman laser, the wavelength of the high-gain-band Ti:sapphire laser was efficiently shifted to the long-wavelength low-gain region with the SRS process, and high-performance Stokes operation was achieved in the original long-wavelength low-gain region of the Ti:sapphire laser. With the fundamental wavelength tuning from 870 to 930 nm, first-order Stokes output exceeding 2.5 W was obtained at 930–1000 nm, which was significantly higher than that directly generated by the Ti:sapphire laser; furthermore, it exhibited improved beam quality, as well as shorter pulse duration and narrower linewidth. In addition, to the best of our knowledge, the self-mode-locked modulations of first- and second-order Stokes generation were observed for the first time in Ti:sapphire intracavity solid Raman lasers.

2. Experimental setup

The experimental setup of the high-performance high-gain-band Ti:sapphire intracavity Raman laser operating in the 930–1000 nm low-gain region of the Ti:sapphire laser is shown in Figure 1. The primary pump source was a 10 kHz frequency-doubled neodymium-doped yttrium aluminium garnet (Nd:YAG) pulsed laser at 532 nm, with a maximum output power of 42.1 W and spectral linewidth of 0.1 nm. The corresponding pulse duration and beam quality (M^2) were 69 ns and 19, respectively. A double-end pumping scheme was adopted to reduce the thermal effects of the crystals[10,18]. Two pump beams divided by a half-wave plate (HWP_2) and a polarized beam splitter (PBS_2) in a ratio of 1:1 were focused onto the front and rear facets of the Ti:sapphire crystal by lenses f_1 and f_2 (f = 200 mm) with a radius of 250 μm. When the pump power was 42.1 W, the equivalent thermal focal length of the double-end-pumped crystal was 90 mm.

An elaborately designed symmetrical flat Ti:sapphire cavity was employed to further reduce the influence of the thermal effect on the resonator stability and optimize the output mode. The geometric distances from the M_6 mirror to the front facets of the Ti:sapphire crystal and M_7 mirror to the rear surface of the Ti:sapphire crystal were both 120 mm. A 0.20% (mass fraction) doped Ti:sapphire crystal with dimensions of 4 mm × 4 mm × 15 mm and high figure of merit (FOM > 150) was cut at a Brewster angle at both end facets, wrapped with indium foil and tightly mounted on a copper holder water-cooled at 12°C. HWP_3 and HWP_4 were rotated to adjust the polarization of the pump wave and achieve maximum absorption of the crystal (approximately 90%). A dense flint-glass prism with an apex angle of 60°

https://doi.org/10.1017/hpl.2024.40 Published online by Cambridge University Press

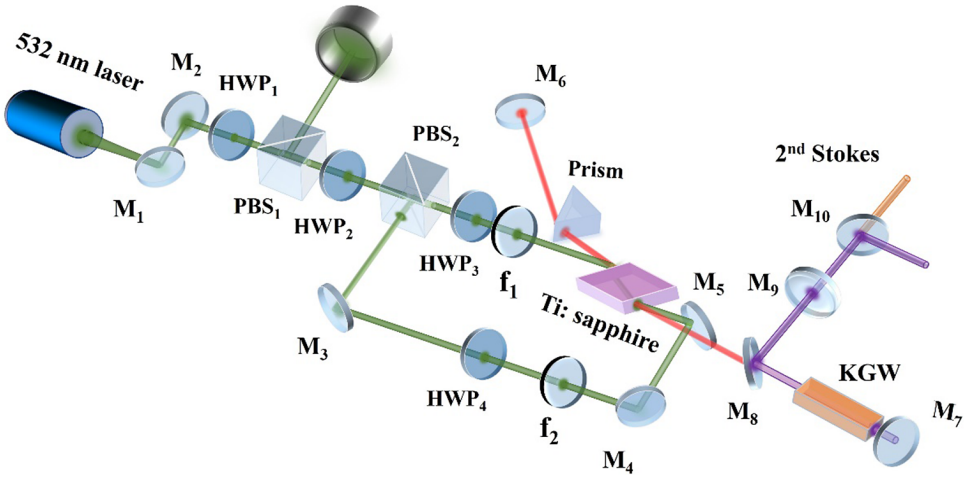

Figure 1. Schematic of the high-performance high-gain-band Ti:sapphire intracavity Raman laser operating in the 930–1000 nm low-gain region of the Ti:sapphire laser.

Table 1. Coatings of mirrors.

Mirrors	Coatings
M_1, M_2, M_3, M_4	45° 532 nm high reflectivity (HR)
M_5	45° 532 nm HR, 45° 700–1000 nm high transmittance (HT)
M_6, M_7	700–1000 nm HR
M_{7*} (OC)	700–1000 nm $T = 40\%$
M_8	45° 790–810 nm HT, 45° 840–870 nm HR
M_{8*}	45° 840–890 nm HT, 45° 900–960 nm HR
M_{8**}	45° 890–930 nm HT, 45° 960–1000 nm HR
M_9 (OC)	850–1000 nm @ $T = 30\%/40\%/50\%/60\%$
M_{10}	M_{8*}/ M_{8**}/900–970 nm HR, 1000–1100 nm HT/950–1000 nm HT, 1050–1100 nm HR

was inserted into the cavity to tune the wavelength of the fundamental waves.

A dichroic mirror, M_8 (M_{8*}, M_{8**}), was inserted into the Ti:sapphire cavity to construct an L-shaped Raman cavity using the M_7 and M_9 mirrors. An *Np*-cut potassium gadolinium tungstate (KGW) Raman crystal with dimensions of 5 mm × 5 mm × 30 mm was polished on both parallel faces and tilted at an angle of 1° to reduce the effect of the undesired satellite cavity. The *Ng* axis of the KGW crystal was parallel to the polarization direction of the fundamental wave. The geometric distance from the rear surface of the KGW crystal to the M_7 mirror was 10 mm and the total geometric length of the Raman cavity was 110 mm. The OC M_9 was a concave mirror with a radius of curvature of 150 mm. The calculated fundamental-mode beam radius of the fundamental and Stokes wave in the Raman crystal is 110 and 120 μm, respectively. The M_{10} mirror served as a dichroic mirror to separate the first- and second-order Stokes lights. All the other mirrors were flat, and their coatings are listed in Table 1. In our experiment, the optical power was measured using an Ophir NOVA II laser power meter, and the pulse shapes were recorded using fast photodetectors (Max-Ray Photonics PD12D, Thorlabs DET10A) and an oscilloscope (Agilent DSO9254A). The central wavelength and spectral linewidth were measured using an optical spectrum analyser (Yokogawa AQ6370D).

3. Rate equation model

Based on the coupled rate equations of the Ti:sapphire lasers[19], the theoretical model of the narrow-linewidth Ti:sapphire folded-coupled intracavity Raman lasers can be established using the following coupled rate equations[20]:

$$\frac{\mathrm{d}n}{\mathrm{d}t} = S_\mathrm{P}(t) - \frac{c\sigma n\phi_\mathrm{L}}{n_\mathrm{T}} - \frac{n}{\tau}, \tag{1}$$

$$\frac{\mathrm{d}\phi_\mathrm{L}}{\mathrm{d}t} = \frac{c\sigma n\phi_\mathrm{L} l_\mathrm{L}}{n_\mathrm{T} L_\mathrm{L}} - \frac{\phi_\mathrm{L}}{\tau_\mathrm{L}} - \frac{2g_\mathrm{eff} hc^2 \phi_\mathrm{S}\phi_\mathrm{L} l_\mathrm{S}}{\lambda_\mathrm{L} t_\mathrm{L} n_\mathrm{K}}, \tag{2}$$

$$\frac{\mathrm{d}\phi_\mathrm{S}}{\mathrm{d}t} = \frac{2g_\mathrm{eff} hc^2 \phi_\mathrm{S}\phi_\mathrm{L} l_\mathrm{S}}{\lambda_\mathrm{S} t_\mathrm{S} n_\mathrm{K}} - \frac{\phi_\mathrm{S}}{\tau_\mathrm{S}}, \tag{3}$$

$$S_\mathrm{P}(t) = \frac{2\sqrt{\ln 2}\eta P_0 \lambda_\mathrm{p}}{\pi\sqrt{\pi} f_\mathrm{p} T_0 hc\omega_\mathrm{p}^2 l_\mathrm{L}} \exp\left[-\left(\frac{2\sqrt{\ln 2}}{T_0} t\right)^2\right], \tag{4}$$

$$\tau_{\mathrm{L,S}} = \frac{t_{\mathrm{L,S}}}{\alpha_{\mathrm{L,S}} - \ln\left(R_{\mathrm{L,S}}\right)} = \frac{2L_{\mathrm{LO,SO}}}{c\left[\alpha_{\mathrm{L,S}} - \ln\left(R_{\mathrm{L,S}}\right)\right]}, \tag{5}$$

where n is the inversion population density; ϕ_L and ϕ_S are the average photon densities inside the laser and Stokes cavity, respectively; and λ_p, λ_L and λ_S are the pump, laser and Stokes wavelengths (532, 800 and 852.9 nm), respectively. To simplify the theoretical model, the aforementioned coupled rate equations ignore higher-order Stokes waves.

For the narrow-linewidth Ti:sapphire folded-coupled intracavity Raman lasers, the fundamental and Stokes wave can be considered as mutually independent, despite both being

https://doi.org/10.1017/hpl.2024.40 Published online by Cambridge University Press

located within the emission band of a Ti:sapphire laser. This premise serves as the foundational basis upon which the aforementioned theoretical model is constructed. In addition, for broad laser fields with a bandwidth larger than the spontaneous Raman linewidth ($\Delta\omega_L > \Delta\omega_R$), the effective Raman gain g_{eff} differs from the monochromatic Raman gain coefficient g_0, which depends on the level of dispersion, fundamental bandwidth and fundamental intensity[21]. Using Equation (3.25) in Spence's work[22], the g_{eff} used in the subsequent calculations was calculated to be only approximately 40% of g_0. By further narrowing the spectral linewidth of Ti:sapphire lasers with high-resolution dispersion elements such as gratings and etalons, the g_{eff} can be further increased and gradually approach g_0.

Based on the parameters listed in Table 2, the coupled rate equations (1)–(5) can be solved numerically as follows. The simulated temporal evolutions of the residual laser photon density ϕ_L and Stokes photon density ϕ_S are shown in Figure 2(a). When the pump power P_0 is 42 W and OC $R_S = 50\%$, the calculated pulse durations of the Stokes and residual laser waves are 1.91 and 8.39 ns, respectively. According to Equation (6)[20], the output Stokes powers with various OC reflectivities are calculated, as shown in Figure 2(b). The threshold pump power decreases with increasing R_S. When the pump power is 42 W and the optimal OC reflectivity R_S is 50%, with a maximum output power of 6.24 W at 852.9 nm. However, the actual output Stokes power measured in experiments should be lower than the simulated results, accompanied by larger pulse duration, because higher-order mode operations are neglected owing to the poor pump beam quality M^2 and the thermal effects of the crystal:

$$P_{L,S} = \frac{f_p c^2 \pi \omega_{L,S}^2 h}{2\lambda_{L,S}} \ln\left(\frac{1}{R_{L,S}}\right) \int_0^{t_b} \phi_{L,S} dt. \quad (6)$$

The maximum output powers of the narrow-linewidth Ti:sapphire and Raman lasers at different wavelengths were calculated according to the stimulated emission cross-sectional curve of the Ti:sapphire crystal[23], as shown in Figure 3. For Ti:sapphire lasers, each wavelength attains its maximum output power at an optimal transmittance, which gradually decreases as the wavelength shifts from the central wavelength. Oscillations at wavelengths greater than 1000 nm are a challenge for Ti:sapphire lasers. In contrast,

Table 2. Related parameters used in calculations[23,24].

Symbol	Parameter	Value
h	Planck constant	6.626×10^{-34} J s
c	Light velocity in the vacuum	3×10^8 m/s
l_L	Length of gain medium (Ti:sapphire crystal)	13 mm
l_S	Length of Raman crystal (KGW crystal)	30 mm
n_T	Refractive index of gain medium	1.7602 @ 800 nm
n_K	Refractive index of Raman crystal	1.99 @ 852.9 nm
σ	Stimulated emission cross-section of gain medium	3×10^{-23} m^2 @ 800 nm
τ	Fluorescent lifetime in upper level of gain medium	3.2 μs
ω_p	Pump beam radius in gain medium	0.25 mm
ω_L	Average radius of Ti:sapphire laser in cavity	0.25 mm
ω_S	Average radius of Stokes wave in cavity	0.16 mm
L_L	Length of laser cavity	253 mm
L_S	Length of Raman cavity	110 mm
η	Pump absorption ratio of gain medium	88%
f_p	Pulse repetition rate of the pump wave	10 kHz
T_0	Pulse duration of the pump wave	69 ns
P_0	Maximum input pump power	42 W
R_L	Output coupler reflectivity at laser wavelength	0.99
R_S	Output coupler reflectivity at Stokes wavelength	
α_S	Roundtrip dissipative optical loss of Stokes wave	0.04
α_L	Roundtrip dissipative optical loss of laser	0.06
g_0	Line-centre monochromatic Raman gain coefficient	4.4 cm/GW
g_{eff}	Effective Raman gain coefficient	$0.4g_0$

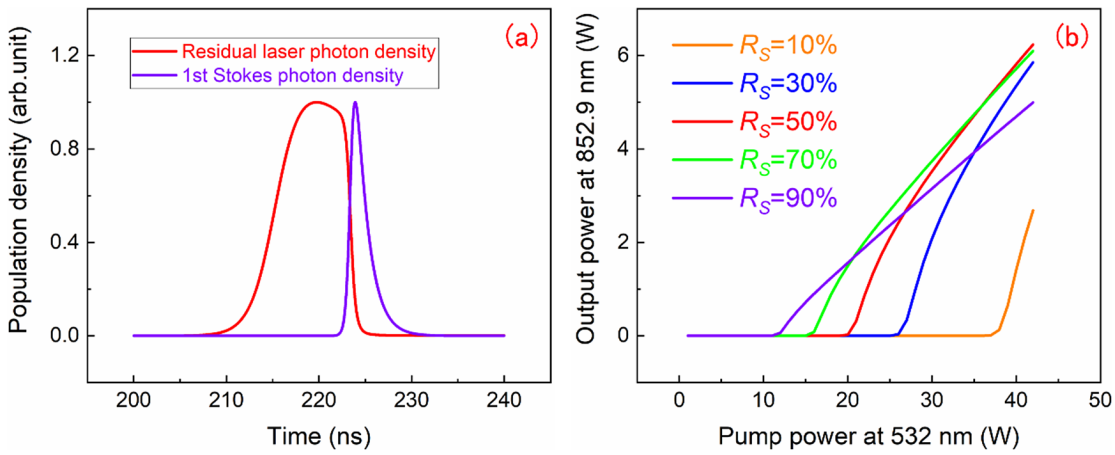

Figure 2. (a) Pulse establishment of the Ti:sapphire Raman laser. (b) Simulated Stokes power transfer for various OC reflectivities.

https://doi.org/10.1017/hpl.2024.40 Published online by Cambridge University Press

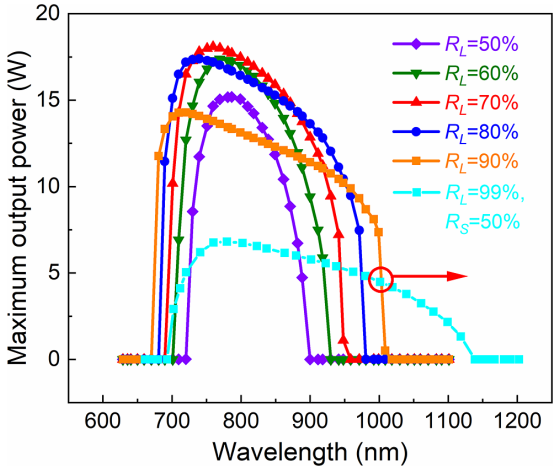

Figure 3. Maximum output powers of the narrow-linewidth Ti:sapphire and Raman lasers with various OC reflectivities.

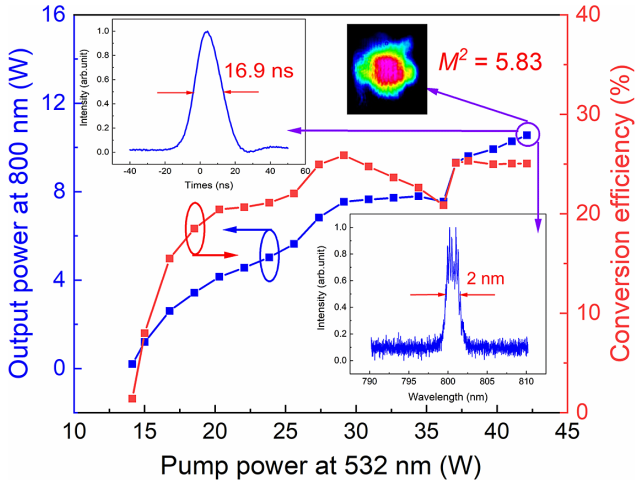

Figure 4. Power transfer and conversion efficiency at 800 nm. Inset: measured fine spectrum, pulse duration and beam quality at 10.55 W.

the Ti:sapphire Raman laser can achieve high-power laser operation in the range of 1000–1200 nm, although its power performance in the 800–900 nm range is inferior to that of the Ti:sapphire laser. The calculations demonstrated the potential of Ti:sapphire Raman lasers to replace Ti:sapphire lasers in the 1000–1200 nm low-gain region. In addition, the practical output powers of the Ti:sapphire and Raman lasers were lower than the calculated results owing to neglecting the mode mismatch caused by the thermal effects of the crystal. Therefore, the power advantage region of Ti:sapphire Raman lasers may be further expanded towards the short-wavelength region.

4. Results and discussion

4.1. High-repetition-rate Ti:sapphire laser

In this experiment, the KGW Raman crystal and dichroic mirror M_8 were removed from the fundamental cavity[21]. The M_7 mirror was replaced with the OC M_{7*} (T = 40% @ 700–1000 nm) to investigate the output performance of the high-repetition-rate Ti:sapphire laser at the central wavelength of 800 nm. The power transfer and conversion efficiencies are shown in Figure 4. The threshold pump power of the Ti:sapphire laser at 800 nm was 14.1 W. When the pump power was 42.1 W, a maximum output power of 10.55 W and a linewidth of 2 nm were obtained at 800 nm. The corresponding conversion efficiency was 25%. The measured output pulse duration was 16.9 ns and the beam quality M^2 was 5.83, as shown in Figure 4. Due to the effective thermal management of the Ti:sapphire crystal by the dual-end pumping scheme and the elaborate symmetrical flat cavity design, higher output power can be obtained with a further increased pump power, and the beam quality of the Ti:sapphire laser is significantly better than that of the pump light.

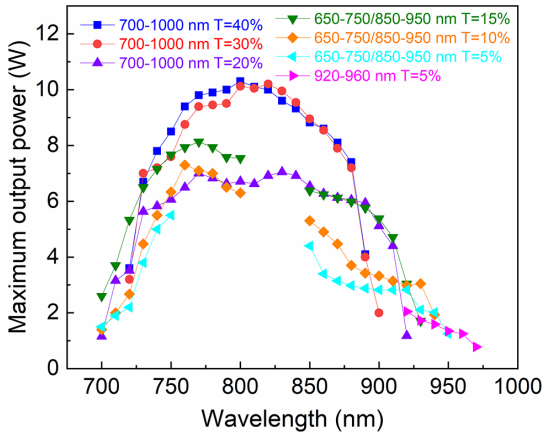

Figure 5. Maximum output power at 700–970 nm for various OC transmittances.

The maximum output power of the Ti:sapphire laser in the wavelength coverage of 700–970 nm was obtained for various transmittances of the M_{7*} mirror, as shown in Figure 5. Notably, each output wavelength possesses its own optimal transmittance for attaining the maximum output power. For the OC transmittance varying from 20% to 40%, tunable laser output exceeding 3 W can be obtained at wavelengths of 710–930 nm, which is the high-gain region of the described Ti:sapphire laser. The power reduced significantly as the output wavelength gradually shifted from the high-gain region of the Ti:sapphire laser. When the output wavelength was 970 nm, the maximum output power was only 0.78 W. As mentioned in the introduction, this significant reduction was caused by the rapid decreased emission cross-section in the low-gain region of the Ti:sapphire laser, which was consistent with our simulation results in Figure 3. However, unlike the simulated results in Figure 3, not all the measured powers in Figure 5 were obtained at a maximum pump power of 42.1 W. The increased reflectivity of the OC leads to

https://doi.org/10.1017/hpl.2024.40 Published online by Cambridge University Press

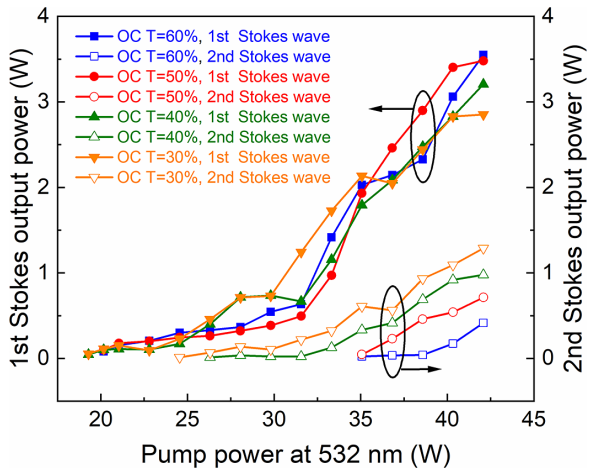

Figure 6. Power transfer of first- and second-order Stokes waves for various OC transmittances.

a stronger absorption of the oscillating wave in the cavity by the Ti:sapphire crystal, thereby intensifying the thermal effect of the crystal. Hence, to achieve stable laser operation with a low OC transmittance ($T \leq 20\%$), the pump power must be reduced, which was not considered in our previous simulations in Figure 3.

4.2. Ti:sapphire intracavity Raman laser (fundamental wavelength: 800 nm)

The operating wavelength of the Ti:sapphire laser was maintained at 800 nm and OC M_{7*} was replaced by the M_7 mirror. A dichroic mirror M_8 and KGW Raman crystal were inserted into the laser cavity to construct a folded Raman cavity. The power transfer of the first- and second-order Stokes waves was investigated by varying the transmittance of OC M_9, as shown in Figure 6. The threshold pump power for the first-order Stokes generation was 19.2 W for an OC transmittance of 30%. As the pump power increased, second-order Stokes generation was observed at a threshold pump power of 24.5 W. The threshold pump power of the second-order Stokes generation increased significantly with the transmittance of OC M_9, owing to a higher oscillating loss. When the pump power increased to 42.1 W, the first-order Stoke output powers of 2.85, 3.2, 3.48 and 3.55 W were obtained with the OC transmittances of 30%, 40%, 50% and 60%, respectively, while the corresponding second-order Stokes output powers were 1.2, 0.98, 0.72 and 0.42 W, respectively. With an OC transmittance of 50%, a maximum total Stokes output power of 4.2 W was achieved with a conversion efficiency of 10%. A higher first-order Stokes output power was obtained by increasing the transmittance of OC M_9 to the second-order Stokes wave.

The Stokes wave spectra were measured at a maximum pump power of 42.1 W for an OC transmittance of 30%, as shown in Figure 7. The centre wavelengths of the first- and second-order Stokes waves are 852.9 and 912.5 nm, respectively. In fact, the third-order Stokes wave at 981.5 nm was also observed with very weak intensity, indicating a high Raman gain of the KGW crystal. The third-order Stokes wave disappeared at OC transmittances of 50% and 60% owing to the higher oscillating losses of the second-order Stokes wave. The Raman shift was calculated to be 767 cm^{-1}, indicating that the pumping polarization was aligned along the *Ng* axis of the KGW crystal. The fine spectra of the Stokes waves are shown in Figures 7(b)–7(d). The first-order Stokes output linewidth at 852.9 nm was 1 nm, which is significantly smaller than that of the fundamental wave at 800 nm shown in Figure 4. This is mainly because the threshold pump intensity of the first-order Stokes wave limits its oscillation mode. Hence, the cascade Raman process yielded a narrower Stokes linewidth. The second- and third-order Stokes linewidths were 0.5 and 0.35 nm, respectively. Furthermore, this device of the Ti:sapphire Raman laser could achieve efficient high-order Stokes output if the coating of the mirrors was HR for the first- and second-order Stokes waves.

The power transfer and conversion efficiency of the first-order Stokes wave were investigated at an OC transmittance of 60% by rotating the KGW crystal by 90° to align the pumping polarization along the *Nm* axis of the KGW crystal, as shown in Figure 8(a). Lower threshold pump power and higher output power were obtained because of the large Raman gain coefficients g_0 (*Ng*: 4.4 cm/GW, *Nm*: 3.3 cm/GW @ 1064 nm) when the fundamental polarization was along the *Ng* axis[25]. When the pump power was 42.1 W, the first-order Stokes output powers were 3.55 W (*E//Ng*) and 2.95 W (*E//Nm*), respectively, which corresponded to the conversion efficiencies of 8.44% and 7.03%. According to the measured Stokes spectrum shown in Figure 8(b), the Raman shift of the *E//Nm* axis was calculated to be 901 cm^{-1}, which was slightly larger than that of the *E//Ng* axis (767 cm^{-1})[25]. At the same fundamental wavelength (800 nm), the central wavelengths of the first- and second-order Stokes waves were further shifted, reaching 862 and 934.5 nm, respectively. The 901 cm^{-1} shift enables a greater wavelength extension of the Ti:sapphire laser, thereby compensating for its slightly lower Raman gain, and holds a significant advantage in high-order Stokes operation. However, for the first-order Stokes wave, this limited increase in the wavelength shift (~10 nm) made it difficult to offset the gain gap. Therefore, subsequent experiments aligned the pumping polarization along the *Ng* axis of the KGW crystal.

4.3. Ti:sapphire intracavity Raman laser operating in the 930–1000 nm low-gain region

The above experiments demonstrated the excellent Stokes output performance of the Ti:sapphire intracavity Raman

https://doi.org/10.1017/hpl.2024.40 Published online by Cambridge University Press

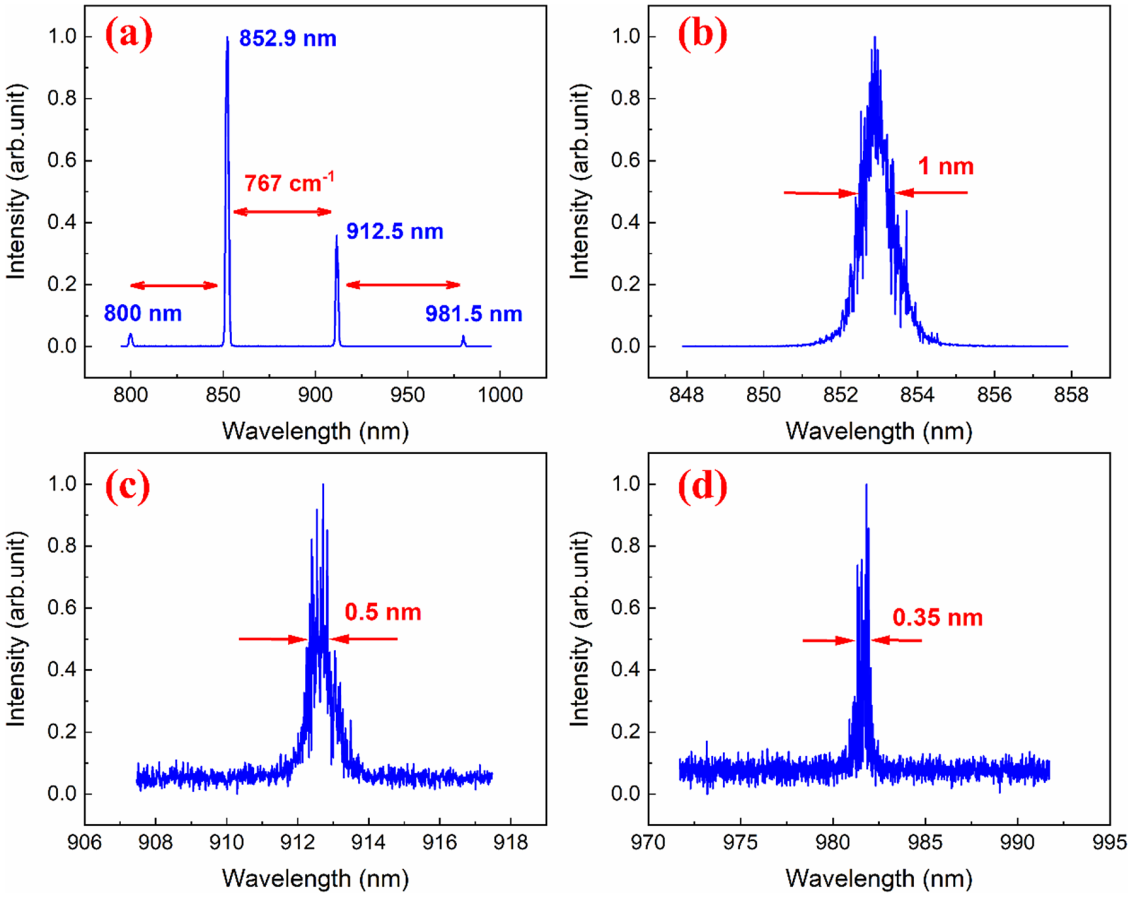

Figure 7. Measured fine spectrum of Stokes waves with OC transmittance of 30%.

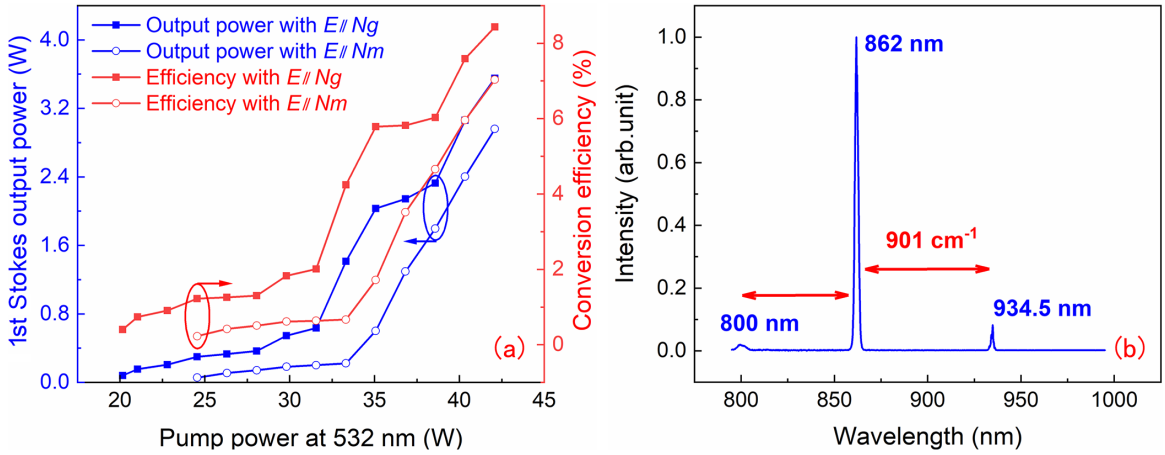

Figure 8. (a) Power transfer and conversion efficiency of first-order Stokes wave with OC transmittance of 60%. (b) Measured fine spectrum of Stokes waves of the *E//Nm* axis.

laser. However, the output power of the Ti:sapphire intracavity Raman laser in the 930–1000 nm low-gain region of the Ti:sapphire laser was of greater interest. By adjusting the M_6 mirror and replacing the dichroic mirror M_8 with M_{8}^{**}, the first-order Stokes output at 960 nm and the second-order Stokes output at 1036.5 nm can be obtained with a fundamental wavelength of 894 nm. The power transfer and conversion efficiencies of the Stokes outputs for various OC transmittances are shown in Figure 9. Compared with the Stokes output powers shown in Figure 6, the threshold pump powers of both the first- and second-order Stokes waves increased, while the maximum Stokes output power and the optimal OC transmittances both decreased. This is undoubtedly due to the reduced gain of the fundamental

https://doi.org/10.1017/hpl.2024.40 Published online by Cambridge University Press

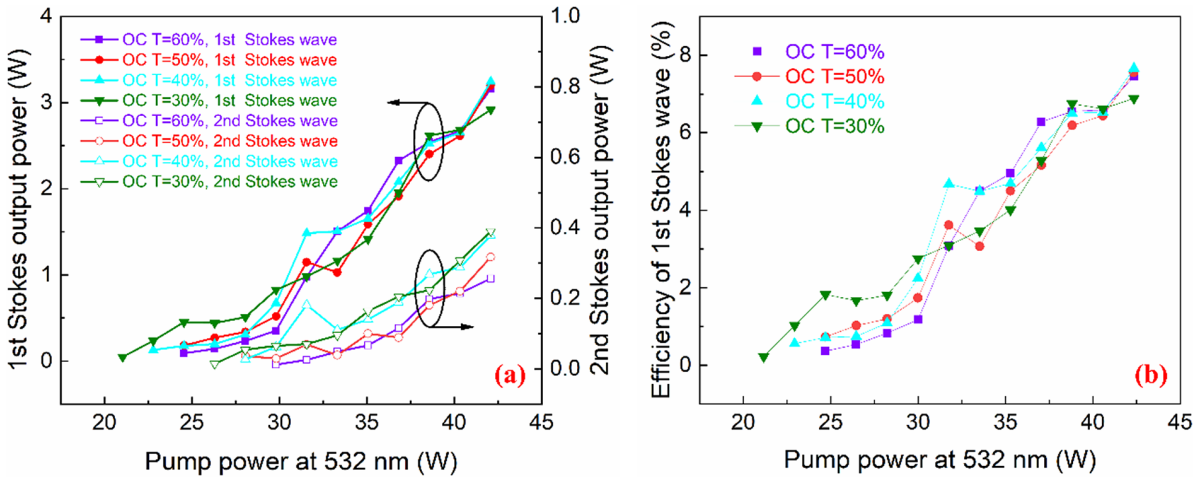

Figure 9. (a) Power transfer and (b) conversion efficiency of the Stokes outputs with various OC transmittances.

Figure 10. Mode-locked modulations of the (a) first-order Stokes pulses (3.24 W), (b) second-order Stokes pulses (0.39 W) and (c) first-order Stokes pulses (near threshold).

wavelength at 894 nm, owing to its distance from the central wavelength at 800 nm. When the pump power was 42.1 W, with OC transmittances of 30%, 40%, 50% and 60%, the first-order Stokes output powers were 2.92, 3.24, 3.2 and 3.16 W, respectively, while the corresponding optical-to-optical conversion efficiencies were 6.88%, 7.66%, 7.55% and 7.45%, respectively. At an OC transmittance of 30%, the maximum second-order Stokes output power at 1036.5 nm was 0.39 W. The maximum first-order Stokes output power obtained at 960 nm (3.24 W) in this device was significantly higher than that directly generated by the Ti:sapphire laser shown in Figure 5 (1.25 W). Thus, this device can achieve efficient laser operation in the long-wavelength low-gain region of the Ti:sapphire laser.

The first- and second-order Stokes pulse shapes were recorded using a high-speed photodetector (Max-Ray Photonics PD12D) and an oscilloscope (Agilent DSO9254A). The mode-locked modulations of the first- and second-order Stokes pulses were observed, as shown in Figure 10. The pulse duration of the 960 nm first-order Stokes gain-switched envelope was 4.7 ns, and the modulation depth of the mode-locked first-order Stokes pulse was approximately 40%. In contrast, the modulation depth of the mode-locked 1036.5 nm second-order Stokes pulse reached 100%, and the pulse duration of the second-order Stokes envelope was approximately 2.1 ns. Four mode-locked pulses were observed in the second-order Stokes gain-switched envelope, and the pulse repetition frequency (PRF) was 1.07 GHz, corresponding to the roundtrip time of the second-order Stokes wave in the Raman resonator (0.93 ns). The mode-locked pulse duration measured on the oscilloscope was 178.66 ps. The mode-locked pulse duration can be estimated by the following equation[26]:

$$\tau_{\text{real}} = \sqrt{\tau^2_{\text{measure}} - \tau^2_{\text{probe}} - \tau^2_{\text{oscilloscope}}}, \tag{7}$$

$$\tau_{\text{oscilloscope}} \times \text{BW} = 0.35 - 0.4, \tag{8}$$

where τ_{real} is the real pulse rise time, τ_{measure} is the measured pulse rise time and τ_{probe} is the rise time of the probe (18 ps). The rise time of oscilloscope $\tau_{\text{oscilloscope}}$ is determined by Equation (8), where the BW is the bandwidth of the oscilloscope. The bandwidth of the oscilloscope in our experiment is 2.5 GHz, corresponding to a rise time of 140 ps. According to the definition of the rise time and considering the symmetric shape of the mode-locked pulse, we can assume the mode-locked pulse width is approximately 1.25 times of the real rise time. Hence, the

https://doi.org/10.1017/hpl.2024.40 Published online by Cambridge University Press

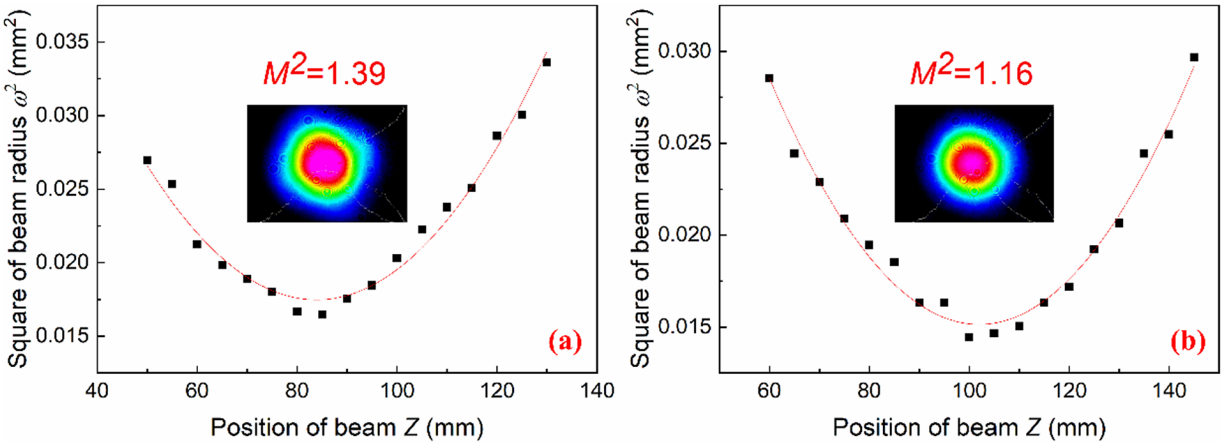

Figure 11. Beam quality at the maximum output powers of 960 and 1036.5 nm with an OC transmittance of 40%.

rise time of the mode-locked pulse $\tau_{measure}$ was calculated to be 142.9 ps and the estimated duration of the second-order Stokes mode-locked pulse was less than 28 ps.

Such a narrow second-order Stokes gain-switched envelope and mode-locked pulse duration were due to pulse duration compression by the cascade Raman process. The mode locking mechanism of Stokes wave is similar to that of the Kerr effect[27]. The co-oscillation of the fundamental and Stokes wave within the Raman crystal induces an enhancement in refractive index, leading to an intensity modulation caused by the self-focusing of the fundamental and Stokes wave within the Raman crystal. The modulation depth of the first-order Stokes pulse was significantly lower than that near the thershold because the self-mode locking of the first-order Stokes pulse was destroyed by the depletion of its radiation when the second-order Stokes pulse was generated[28]. The modulation depth of the first-order Stokes pulse can be significantly improved by optimizing the transmittance of the OC to suppress second-order Stokes generation. In addition, the PRF of second-order mode-locked pulses varied only with the length of the Raman cavity, confirming the existence of a mode-locking regime in the Raman laser[22,27–30]. To the best of our knowledge, the self-mode-locked modulation of first- and second-order Stokes generation has been observed in Ti:sapphire intracavity solid Raman lasers for the first time. The discovery of the aforementioned mode-locking phenomenon confirms that the SRS self-mode-locking process of SRS is independent of the gain-switching elements.

For an OC transmittance of 40%, the beam qualities of the maximum output power at 960 and 1036.5 nm were measured to be 1.36 and 1.19, respectively, using knife-edge scanning. The Stokes beam qualities in Figure 11 improved significantly compared to that of the fundamental beam ($M^2 = 5.83$) owing to the clean-up effect of the SRS process. In addition, the stability of the first-order Stokes output power at 960 nm was measured within 1 h, as shown in Figure 12. The average power was 3.24 W, with a root-mean-square fluctuation of 1.08%. The output power was relatively stable, which was primarily attributed to the good thermal management. The dual-end pumping scheme and elaborate design of the symmetrical flat cavity ensured stable operation of the laser at higher pump powers.

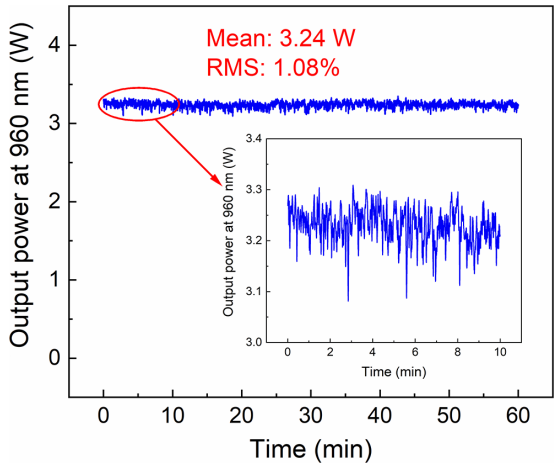

Figure 12. Stability of the first-order Stokes output power at 960 nm within 1 h with an OC transmittance of 40%. Inset: power stability within 10 min.

A 900–1000 nm tunable Stokes output can be achieved through tuning the fundamental wavelength by tilting the mirror M_6. By utilizing the mirror M_{10} to filter the fundamental wave behind the OC M_9, the maximum output power and fine spectra of the first-order Stokes wave in the 900–1000 nm range are shown in Figure 13(a). The first-order Stokes output, which exceeded 2.5 W, was achieved in the 900–1000 nm range (red line). In particular, the maximum first-order Stokes output power in the 920–1000 nm range was significantly higher than that directly generated by the Ti:sapphire laser shown in Figure 5 (green line in Figure 13). Notably, the calculated value of the first-order Stokes output power (pink line in Figure 13) surpasses the

https://doi.org/10.1017/hpl.2024.40 Published online by Cambridge University Press

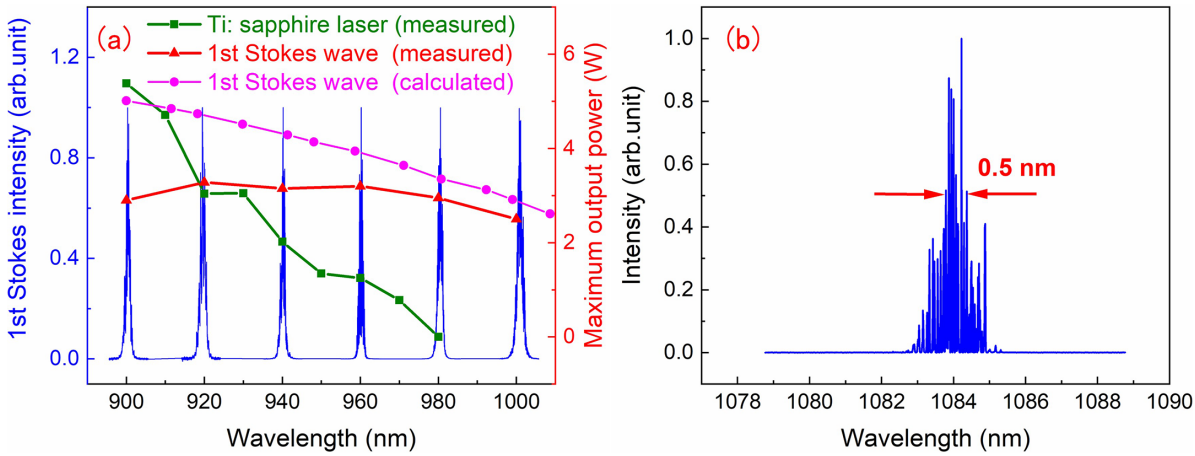

Figure 13. (a) Maximum output powers and fine spectra of the first-order Stokes wave at 900–1000 nm. (b) Fine spectrum of the second-order Stokes wave at 1083.7 nm.

experimental measurement as a whole. This discrepancy arises from overlooking the impact of mode mismatching and higher-order Stokes generation during the calculation. In addition, first-order Stokes output power shows little variation within the range of 900–1000 nm was remarkable. This phenomenon can be primarily attributed to three reasons. Firstly, the difference in the emission cross-sections of the 840–930 nm fundamental wavelength was relatively small. Secondly, the high-reflectivity coating of the M_6 and M_9 mirrors for the fundamental wavelength in the 840–930 nm range effectively enhanced the pump intensity within the cavity, effectively compensating for the gain discrepancy of the fundamental wavelength resulting from the disparity in the emission cross-section. The power at 900 nm seemed to be a little lower according to the trend of the calculated power curve. This was primarily attributed to the additional loss caused by the difference in transmittance between the edge and central regions of the coating on dichroic mirrors M_{8*} and M_{8**}. The maximum output power and first-order Stokes wavelength can be further enhanced by optimizing the coatings of dichroic mirrors M_{8**} and OC M_9. Figure 13(b) presents the output spectrum of a 1083.7 nm second-order Stokes wave with a fundamental wavelength of 930 nm. The second-order Stokes wavelength can also be extended beyond the emission spectrum of the Ti:sapphire by optimizing the coating of the mirrors.

5. Conclusion

A method to improve the output performance of a Ti:sapphire laser in the long-wavelength low-gain region with an efficient SRS process was demonstrated. By making full use of the high pump intensity in the intracavity Raman laser, the wavelength of the high-gain-band Ti:sapphire laser was efficiently shifted to the long-wavelength low-gain region with the SRS process, and high-performance Stokes operation was achieved in the original long-wavelength low-gain region of the Ti:sapphire laser. With the fundamental wavelength tuning from 870 to 930 nm, first-order Stokes output exceeding 2.5 W was obtained at 930–1000 nm, which was significantly higher than that directly generated by the Ti:sapphire laser, accompanied by better beam quality, shorter pulse duration and narrower linewidth. Under the pump power of 42.1 W at 532 nm, a maximum first-order Stokes power of 3.24 W was obtained at 960 nm, with a conversion efficiency of 7.7%. The corresponding linewidth, pulse duration and beam quality were 1 nm, 4.7 ns and 1.39, respectively. In addition, to the best of our knowledge, the self-mode-locked modulation of first- and second-order Stokes generation was observed for the first time in Ti:sapphire intracavity solid Raman lasers. The high-performance long-wavelength low-gain-band Ti:sapphire laser with higher output power is expected to be obtained, through integration with the Ti:sapphire amplification technique.

Acknowledgement

This work was supported by the National Natural Science Foundation of China (No. 62175181).

References

1. S. Tokita, Y. Izawa, H. Niki, and F. Kuwashima, J. Nucl. Sci. Technol. **40**, 1014 (2003).
2. X. Ding, X. Li, Q. Sheng, C. P. Shi, S. J Yin, B. Lin, X. Y. Yu, W. Q. Wen, and J. Q. Yao, Chin. Phys. Lett. **28**, 094205 (2011).
3. G. Wagner, A. Behrendt, V. Wulfmeyer, F. Späth, and M. Schiller, Appl. Opt. **52**, 2454 (2013).
4. Q. S. Zong, Q. Bian, C. Xu, J. Q. Chang, L. J. He, Y. Bo, J. W. Zuo, Y. T. Xu, D. F. Cui, Q. J. Peng, and Z. Y. Xu, Opt. Laser Technol. **113**, 52 (2019).
5. H. Liu, G. Y. Wang, J. W. Jiang, W. L. Tian, D. C. Zhang, H. N. Han, S. B. Fang, J. F. Zhu, and Z. Y. Wei, Chin. Opt. Lett. **18**, 071402 (2020).

https://doi.org/10.1017/hpl.2024.40 Published online by Cambridge University Press

6. T. Takano, H. Ogawa, C. Ohae, and M. Katsuragawa, Opt. Express **29**, 6927 (2021).
7. J. P. Zou, H. Coïc, and D. Papadopoulos, High Power Laser Sci. Eng. **10**, e5 (2022).
8. S. Raeder, A. Hakimi, N. Stöbener, N. Trautmann, and K. Wendt, Anal. Bioanal. Chem. **404**, 2163 (2012).
9. L. P. Zhang, G. L. Guo, F. Q. Li, Z. Shi, and H. D. Lu, Chin. J. Lasers **44**, 1201002 (2017).
10. Y. T. Bai, X. Ding, X. K. Dai, N. Su, P. Lei, G. X. Jiang, X. R. Zhang, X. X. Li, L. Wu, G. Z. Zhang, and J. Q. Yao, Opt. Laser Technol. **163**, 109401 (2023).
11. https://www.coherent.com/lasers/oscillators/chameleon-ultra.
12. J. T. Murray, W. L. Austin, and R. C. Powell, Opt. Mater. **11**, 353 (1999).
13. O. Lux, S. Sarang, O. Kitzler, D. J. Spence, and R. P. Mildren, Optica **3**, 876 (2016).
14. S. H. Ding, X. Y. Zhang, Q. P. Wang, F. F Su, P. Jia, S. Li, S. Z. Fan, J. Chang, S. S. Zhang, and Z. J. Liu, IEEE J. Quantum Electron. **42**, 927 (2006).
15. O. Kitzler, J. Lin, H. M. Pask, R. P. Mildren, S. C. Webster, N. Hempler, G. P. Malcolm, and D. J. Spence, Opt. Lett. **42**, 1229 (2017).
16. M. Li, O. Kitzler, and D. J. Spence, Opt. Express **28**, 1738 (2020).
17. M. Li, O. Kitzler, R. P. Mildren, and D. J. Spence, Opt. Express **29**, 18427 (2021).
18. Y. T. Bai, X. Ding, P. Lei, G. X. Jiang, L. Wu, G. Z. Zhang, and J. Q. Yao, Proc. SPIE **12959**, 1295913 (2023).
19. F. Song, J. Yao, D. W. Zhou, G. Y. Zhang, and J. G. Tian, Appl. Phys. B **72**, 605 (2001).
20. F. F. Su, X. Y. Zhang, Q. P. Wang, S. H. D, P. Jia, S. T. Li, S. Z. Fan, C. Zhang, and B. Liu, J. Phys. D **39**, 2090 (2006).
21. A. T. Georges, Phys. Rev. A **39**, 1876 (1989).
22. D. J. Spence, Prog. Quantum Electron. **51**, 1 (2017).
23. J. M. Eggleston, L. G. Deshazer, and K. W. Kangas, IEEE J. Quantum Electron. **24**, 1009 (1988).
24. K. F. Wall and A. Sanchez, Lincoln Lab. J. **2**, 447 (1990).
25. X. L. Lv, J. C. Chen, Y. J. Peng, Y. B. Long, G. T. Liu, and Y. X. Leng, Opt. Laser Technol. **140**, 107023 (2021).
26. R. P. Yan, Y. Liu, X. D. Li, Y. P. Zhou, H. B. Xu, Y. G. Jiang, X. D. Wu, F. Peng, Q. L. Zhang, R. Q. Dou, and J. Gao, Infrared Phys. Technol. **111**, 10355 (2020).
27. G. X. Huang, Y. Q. Yu, X. H. Xie, Y. F. Zhang, and C. L. Du, Opt. Express **21**, 19723 (2013).
28. V. A. Lisinetskii, D. N. Busko, R. V. Chulkov, A. S. Grabtchikov, P. A. Apanasevich, and V. A. Orlovich, Opt. Commun. **283**, 1454 (2010).
29. Y. T. Bai, X. Din, G. X. Jiang, P. Lei, B. Sun, T. T. Li, X. R. Zhang, X. X. Li, L. Wu, G. Z. Zhang, and J. Q. Yao, Chin. J. Lasers **48**, 1901003 (2022).
30. V. A. Lisinetskii, H. J. Eichler, H. Rhee, X. Wang, and V. A. Orlovich, Opt. Commun. **281**, 2227 (2008).

https://doi.org/10.1017/hpl.2024.40 Published online by Cambridge University Press